Seismic Retrofit of Soft-First-Story Structures Using Rotational Friction Dampers

Mohammad Mahdi Javidan[1] and Jinkoo Kim[2]

Abstract: In this research a seismic retrofit system consisting of a pin-jointed steel frame and rotational friction dampers is developed for the seismic retrofit of reinforced concrete soft-first-story structures, and its efficiency is evaluated through theoretical formulation, cyclic loading test, and analysis of a case study structure. In this system, pin-jointed steel frames are attached to a framed structure at the first story, and a rotational friction damper is installed at each corner of the steel frames. A theoretical formulation is derived for the amplification mechanism of the rotational friction damper and is used to design the geometry of the damper in such a way that its rotation is maximized for a given lateral drift of the structure. The experimental and analysis results show that the proposed system can be used efficiently to prevent the collapse of the case study structure and reduce interstory drift ratios to the code-stipulated limit states.
DOI: 10.1061/(ASCE)ST.1943-541X.0002433.

Author keywords: Seismic retrofit; Soft-first story; Rotational friction dampers; Seismic design.

Introduction

In Korea, many low-rise residential buildings have been built using reinforced concrete (RC) load-bearing wall systems at upper stories supported by columns on the first story, which provides space for a parking lot [Fig. 1(a)] on the first story. Moreover, many such buildings have core walls located far from the center of geometry, which results in planwise irregularity. This type of structure is vulnerable to earthquakes due to the weak first story and plan asymmetry.

The 2016 Gyeongju earthquake and, more recently, the 2017 Pohang earthquake in Korea, of magnitudes 5.8 and 5.4 M_w, respectively, have proven that the low-rise residential buildings with a soft first story are highly prone to severe damage even under minor earthquakes. As can be seen in the photograph in Fig. 1(b), which was taken in the aftermath of the Pohang earthquake, shear failure of columns on the first story was the most common failure mechanism of these structures.

For a structure with a soft ground story, Sahoo and Rai (2013) proposed a retrofit scheme using a hysteretic damper attached to a chevron brace. Agha Beigi et al. (2014) proposed a retrofit scheme using gapped inclined braces attached to columns on the soft story to share the lateral and vertical loads on the columns after reaching a prescribed displacement. They observed that this retrofit system increases the postyield stiffness and ductility while not affecting the lateral resistance (Agha Beigi et al. 2015). Agha Beigi et al. (2015) investigated the repair cost of soft-first-story RC frame structures and showed that the monetary loss of structures with the soft story on the ground level can be reduced using an effective retrofit strategy. Other retrofit techniques, like base isolation, can also be used, but they need further investigation in terms of life cycle costs (Bucher 2009; Weber et al. 2018; Zhou and Chen 2017). Kim and Jeong (2016) proposed a seismic retrofit scheme for planwise asymmetric structures using slit dampers and showed that the retrofit of torsionally irregular structures needs to be carried out in such a way that, in addition to increasing the overall lateral strength, the ductility demands at the stiff and the flexible sides become identical.

Many studies have been carried out to investigate increasing the amplification factor of dampers using different schemes such as a toggle-brace-damper system (Hwang et al. 2005), scissor-jack-damper system (Şigaher and Constantinou 2003), seesaw energy dissipation system (Kang and Tagawa 2014), and eccentric lever-arm system (Baquero Mosquera et al. 2016). Some of these systems have been proven efficient and applied to real structures.

In the present research, a seismic retrofit scheme is presented for soft-first-story structures, which consists of a pin-jointed steel frame attached to a bay and two rotational friction dampers at the corners of the steel frame. A rotational friction damper is developed in such a way that the amplification factor of the damper rotation is maximized for a given lateral drift. As a result, the proposed rotational friction dampers are effective in terms of energy dissipation capability. The behavior of the damper is formulated and an experimental study carried out to verify the energy dissipation capability of the damper. The proposed retrofit scheme is then applied to the seismic retrofit of a case study structure, and the results are compared with those of the bare structure in terms of maximum and average interstory drift ratios, residual drifts, and asymmetrical behavior.

Proposed Retrofit Scheme

Description

Rotational friction dampers are versatile energy dissipation devices that are applied in various schemes. Previously, Martinelli and Mulas (2010) presented a rotational friction damper that is installed at beam-column joints in precast concrete structures [Fig. 2(a)].

[1]Research Assistant, Dept. of Civil and Architectural Engineering, Sungkyunkwan Univ., Suwon 16419, Korea. ORCID: https://orcid.org/0000-0002-1206-0575. Email: javidan@skku.edu

[2]Professor, Dept. of Civil and Architectural Engineering, Sungkyunkwan Univ., Suwon 16419, Korea (corresponding author). ORCID: https://orcid.org/0000-0002-3605-8189. Email: jkim12@skku.edu

Note. This manuscript was submitted on December 25, 2018; approved on March 26, 2019; published online on October 9, 2019. Discussion period open until March 9, 2020; separate discussions must be submitted for individual papers. This paper is part of the ***Journal of Structural Engineering***, © ASCE, ISSN 0733-9445.

Fig. 1. Common type of soft-first-story structure in Korea: (a) overall configuration; and (b) failure mode of columns. (Images by Jinkoo Kim.)

Lee and Kim (2015) and Lee et al. (2017) used rotational friction dampers in conjunction with steel plate slit dampers for seismic retrofit of moment framed structures. They were also applied to industrial portal frames with an additional recentering device developed by Belleri et al. (2017), as shown in Fig. 2(b). It is seen that these devices are used in hinged portal frames, and the rotation at the friction face is equal to the drift ratio of the structure. Seismic retrofit systems using devices with a recentering effect have been recently developed (Belleri et al. 2017; Naeem et al. 2017; Naeem and Kim 2018; Yousef-Beik et al. 2018), in which the recentering capability restores the structure back to its original position and reduces or eliminates residual deformations after seismic excitation.

In this study, an attempt is made to develop a new seismic retrofit scheme appropriate for soft-first-story structures. Because the first story is softer than the other stories, it is most effective to install the seismic retrofit system on the first story. So as not to block the open space required for parking, dampers are installed at beam-column joints. Because these RC structures have rigid beam-column connections, it is not effective to attach dampers directly to RC beams and columns owing to the minute relative rotation at rigid beam-column joints. Therefore, in this study, the dampers are installed in a pin-jointed steel frame that is attached to the existing structure. Because the relative displacement imposed on a damper located at the corner is not large, an amplification mechanism is applied to achieve an acceptable energy dissipation capacity. Fig. 3 shows the retrofit system proposed in this study. A pin-jointed steel frame is attached to the considered bay of the structure in parallel to the existing columns, and the rotational friction dampers are installed at corners like knee braces. Since the steel frame is pin-jointed, connecting the dampers to the steel frame provides enough relative displacement to dissipate energy. As a result of the amplification mechanism, large axial forces are developed in the damper links, and thus it can impose a large

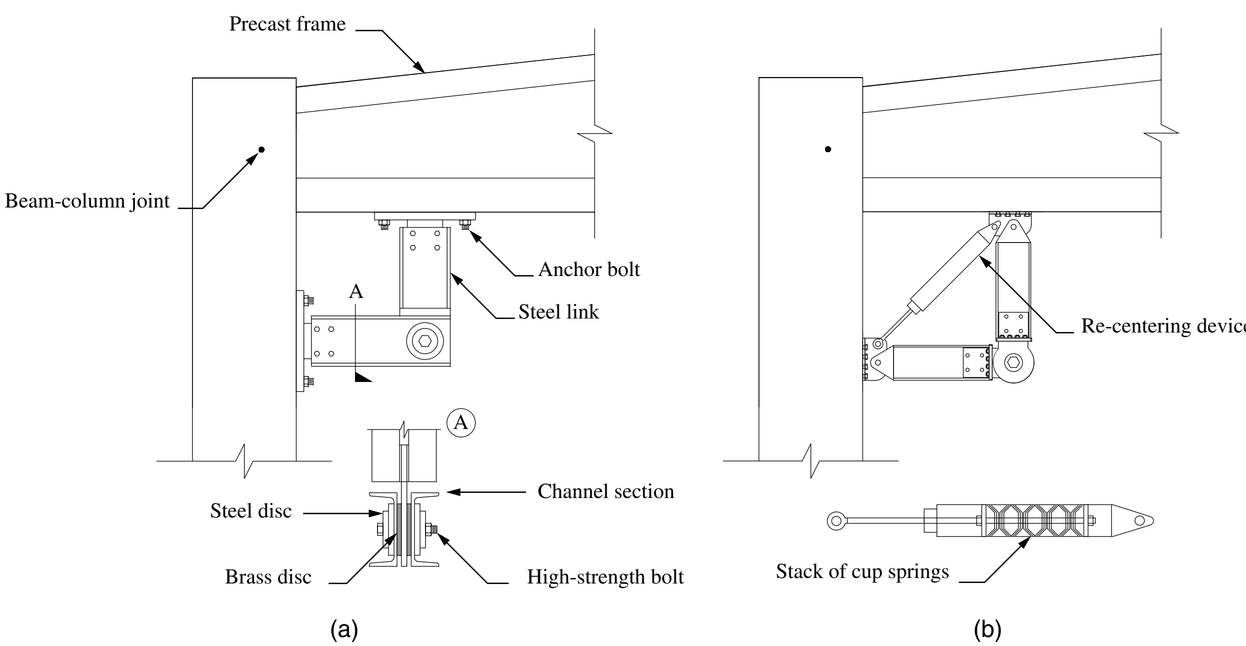

Fig. 2. Previously developed energy dissipation devices placed at beam-column joints: (a) rotational friction device (adapted from Martinelli and Mulas 2010); and (b) recentering device (adapted from Belleri et al. 2017).

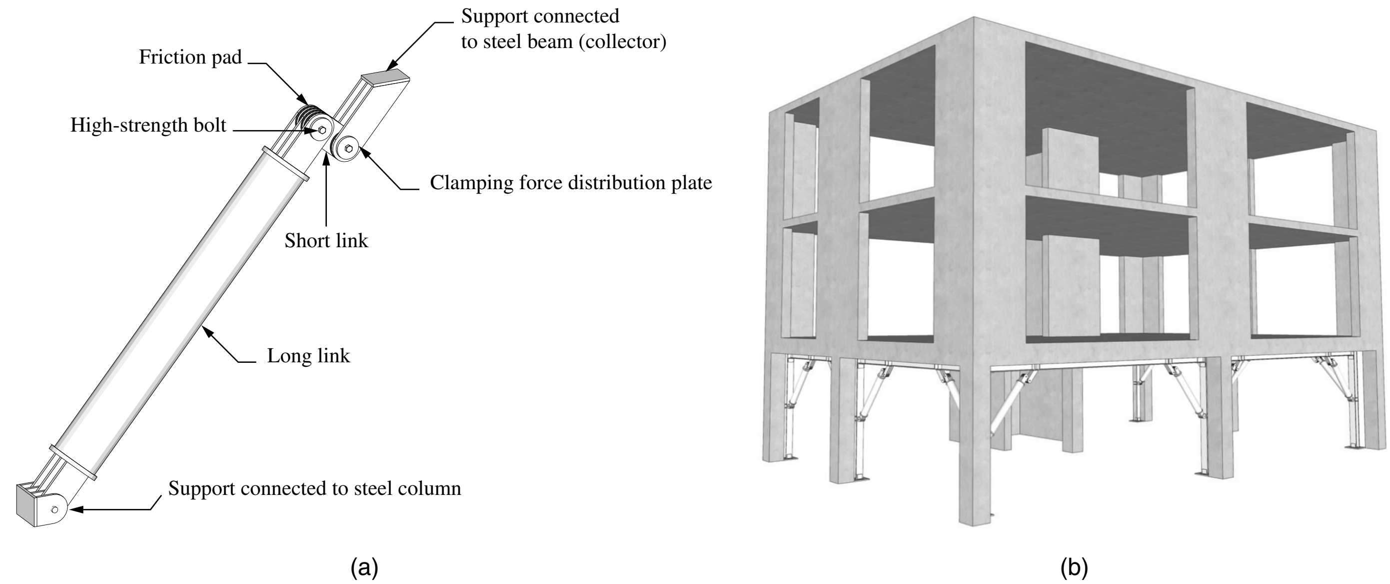

Fig. 3. Proposed retrofit system: (a) details of damper; and (b) installation scheme.

shear force on the existing RC column if it is not connected to the steel frame. The steel beam is attached to the RC beam or the slab using chemical anchors, and this adds stiffness to the existing member, acting as a collector. Therefore, the large axial force induced by the damper is not applied to RC beams as a point load but is applied evenly along the bay. In addition, the steel frame can act as a fail safe, withstanding vertical loads in the case of failure of RC columns. The main advantage of the developed damper is that much larger rotations can be achieved at the friction faces compared with the conventional rotational friction dampers, and, owing to the amplification mechanism, the energy dissipation can be greater for the same lateral drift.

Theoretical Formulation

The relation between the drift ratio and the damper rotation can be formulated using different approaches. As this relation is highly nonlinear, a closed-form solution can be derived more easily using plastic analysis when the yield mechanism forms. A free-body diagram of the retrofit system is depicted in Fig. 4. All elements of the damper or the steel frame are pinned to each other except Link CD, which is the support of Link BC and is connected rigidly to the steel beam. Two friction faces are located at Hinges B and C, and it is assumed that they work as plastic hinges at the yield mechanism. To formulate the behavior of the damper more easily, it is considered that the activation moments and rotations at Hinges B and C are the same. At the yield mechanism, the equation of virtual work for the retrofit system is written

$$F_{\text{yield}} \times \theta H = 4 \times M_{\text{yield}} \times \alpha\theta \tag{1}$$

where F_{yield} = force applied to system at yield of friction dampers; H frame height; M_{yield} = activation moment at friction faces; θ = interstory drift ratio; and α = amplification factor, i.e., ratio of plastic hinge rotation to interstory drift ratio. Thus, $\alpha\theta$ is the rotation at the plastic hinges. To find the amplification factor, F_{yield} can be determined as a function of M_{yield} using the free-body diagram of the damper and the equilibrium equations. The moment equilibrium for Link AB is written

$$F_{By} \times L_1 \sin\theta_1 - F_{Bx} \times L_1 \cos\theta_1 + M_{\text{yield}} = 0 \tag{2}$$

Similarly, the equation of moment equilibrium for Link BC is

$$F_{Bx} \times L_2 \sin\theta_2 + F_{By} \times L_2 \cos\theta_2 - 2M_{\text{yield}} = 0 \tag{3}$$

Eqs. (2) and (3) provide

$$F_{Bx} = \frac{M_{\text{yield}}(2L_1 \sin\theta_1 + L_2 \cos\theta_2)}{L_1 L_2 \cos(\theta_1 - \theta_2)} \tag{4}$$

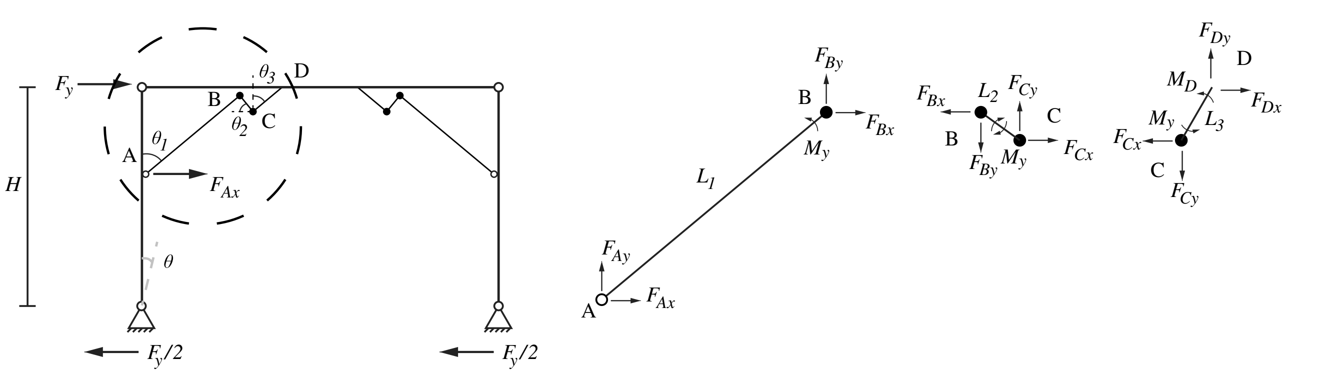

Fig. 4. Free body diagram of rotational friction damper.

$$F_{By} = \frac{M_{\text{yield}}(2L_1 \cos\theta_1 - L_2 \sin\theta_2)}{L_1 L_2 \cos(\theta_1 - \theta_2)} \tag{5}$$

By using F_{Bx} and F_{By}, the axial and shear force acting on each damper element can be found for the design of all the link elements. The horizontal reaction force F_{Ax} acting on the column is equal to F_{Bx}, and therefore the capacity of the system F_{yield} can be found as a function of M_{yield} and the geometry using the equation of moment equilibrium about the pinned corner joint of the frame:

$$\frac{F_{\text{yield}}}{2} \times H = F_{Ax} \times (L_1 \cos\theta_1 - L_2 \sin\theta_1 + L_3 \cos\theta_3) \tag{6}$$

By substituting $F_{Ax} = F_{Bx}$ and F_{yield} into Eq. (1), the amplification factor α is found as

$$\alpha = \frac{(L_1 \cos\theta_1 - L_2 \sin\theta_2 + L_3 \cos\theta_3)(2L_1 \sin\theta_1 + L_2 \cos\theta_2)}{2L_1 L_2 \cos(\theta_1 - \theta_2)} \tag{7}$$

It is observed in Eq. (7) that if one of the links is relatively much shorter than the other, the amplification factor is increased considerably. In this study, Link BC is considered to be the short link. Some constraints and practical issues prevent increasing the amplification factor infinitely. Because of the contact between elements and the required cross-sectional dimensions to withstand the internal forces, it is not possible to decrease the length or the dimensions of the short link as one might wish. To reduce the length of Link BC as much as possible and to prevent the interference of the links during the lateral displacement of the structure, the angles of the links, θ_1 and θ_2, should be equal to each other, and Link BC needs to be perpendicular to Link AB and Link CD. Based on a parametric study, it is observed that practical amplification factors for the proposed retrofit system range from 5 to 7. As previously noted by Baquero Mosquera et al. (2016), practical amplification factors for previously developed retrofit systems with amplification mechanism are between 2 and 8.

In Eq. (7) the amplification factor α is obtained based on the assumption that the rotations at Hinges B and C are the same. However, the exact rotation at each hinge can also be similarly found considering the fact that there is no resisting moment at the other hinge. When this is done, the exact amplification factor and, thus, the rotation at Hinge B are obtained as

$$\alpha_B = \frac{(L_1 \cos\theta_1 - L_2 \sin\theta_2 + L_3 \cos\theta_3)(L_1 \sin\theta_1 + L_2 \cos\theta_2)}{L_1 L_2 \cos(\theta_1 - \theta_2)} \tag{8}$$

and at Hinge C as

$$\alpha_C = \frac{(L_1 \cos\theta_1 - L_2 \sin\theta_2 + L_3 \cos\theta_3)(L_1 \sin\theta_1)}{L_1 L_2 \cos(\theta_1 - \theta_2)} \tag{9}$$

The rotations at Hinges B and C will be identical when either the length of Link BC, L_2, is extremely short or θ_2 is 90°. Because Link BC is considered to be short, currently the difference between the rotations of the two hinges is very small and can be neglected to simplify the calculations. Nevertheless, the capacity F_{yield} obtained by substituting the exact rotations from Eqs. (8) and (9) in Eq. (1) is the same as the capacity found by the amplification factor α derived in Eq. (7). This is due to the fact that the capacity is found using the equilibrium equations, and then α is determined so that it gives the capacity.

Experimental Study

To evaluate the seismic performance of the proposed system, the dampers are tested after being installed at the corners of a pin-jointed steel frame. The design of the dampers is carried out using the formulas derived earlier. The behavior of the damper observed in the test is then assessed using an analysis model of the damper.

Details of the dampers and the installation jig are shown in Fig. 5, and the test setup is shown in Fig. 6. The damper consists of four parts, one support at Hinge A and three links. Link CD is also a support; however, it is elongated to accommodate the displacements of Link BC. The links and supports are made of steel plates with an overall thickness and width of 15 and 100 mm, respectively. Since a large axial force is developed in the longest link, Link AB, which is susceptible to buckling, a pipe section is utilized with an outer diameter of 165.2 mm and thickness of 7.1 mm. Two circular plates with a thickness of 15 mm are welded to both ends of the pipe to close the pipe, and three plates for friction faces are welded on the end plates. There are also three plates at Hinge A and Link CD. Link BC is composed of two plates placed between the three plates of Link AB and Link CD. Based on the formulation presented earlier, the lengths of Links AB, BC, and CD are designed to be 1,500, 125, and 250 mm, respectively, and the damper is installed in the steel frame as shown in Fig. 5. Eight circular friction pads with an outer diameter of 100 mm and inner diameter of 31 mm are used, four pads at each of Hinges B and C. The friction pads are estimated to have a friction coefficient of 0.3. To apply compression force on the friction faces, two high-strength bolts with a diameter of 30 mm and tensile strength of $1.0\ \text{kN/mm}^2$ are used at Hinges B and C. To distribute the clamping force evenly over the friction face, circular plates are inserted between the outer plates and both the bolt head and nut. The bolt pretension is estimated to be on the order of 80 kN based on the torque applied at the assembly. To ensure that the desired clamping force is developed, the bolts are tightened before welding the plates to the pipe. The activation moment of the four friction pads at each hinge with the prescribed bolt pretension can be calculated by (Mualla and Belev 2002)

$$\begin{aligned} M_{\text{yield}} &= N\mu Q\sqrt{0.5(R_i^2 + R_o^2)} \\ &= 4 \times 0.3 \times 80 \times \sqrt{0.5(0.05^2 + 0.015^2)} = 3.5\ \text{kN} \cdot \text{m} \end{aligned} \tag{10}$$

where N = number of friction faces; μ = friction coefficient; Q = clamping force; and R_i and R_o = respectively inner and outer radii of friction face. Using the virtual work and the equilibrium equations for the installation jig and the dampers, the overall capacity of the system is found to be around 25 kN and the amplification factor is 5.7.

Because the proposed damper is a displacement-dependent device, its energy dissipation capability is evaluated using cyclic loading tests. The loading protocol and the force-displacement curve of the retrofit system obtained from the test are shown in Fig. 7. Following the recommendations of ASCE/SEI 41 (ASCE 2013), the loading protocol consists of 10, 5, and 3 fully reversed loading cycles corresponding to 0.25, 0.5, and 1.0 times the device displacement, respectively, under Basic Safety Earthquake-2 (BSE-2X). BSE-2X is defined as the seismic hazard with a 5% exceedance probability in 50 years. As mentioned in ASCE/SEI 41, this seismic hazard is consistent with the maximum considered earthquake (MCE), and for most cases it can be treated as a seismic hazard with a 2% exceedance probability in 50 years. According to the Korean seismic code, the lateral drift of residential structures shall not exceed 1% of the story height under the design basis earthquake and 1.5% under the MCE, which correspond to the

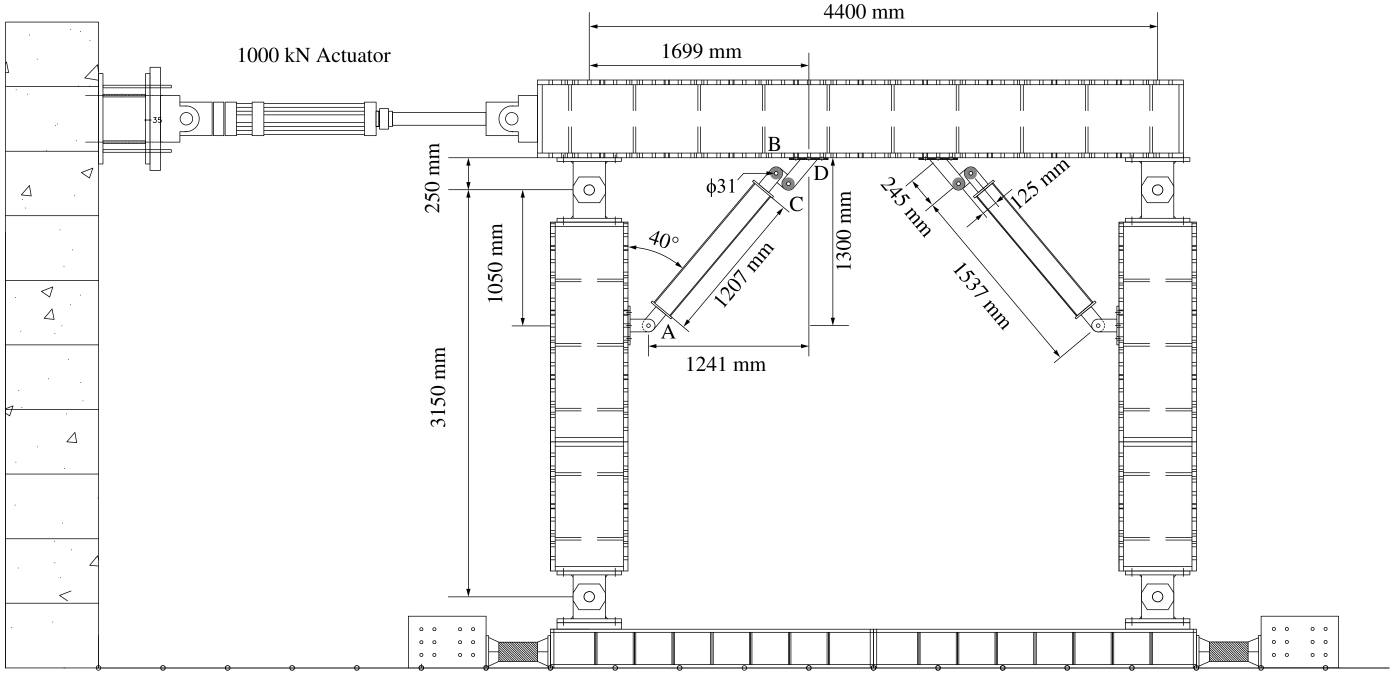

Fig. 5. Details of installation jig.

Fig. 6. Test setup of rotational friction damper.

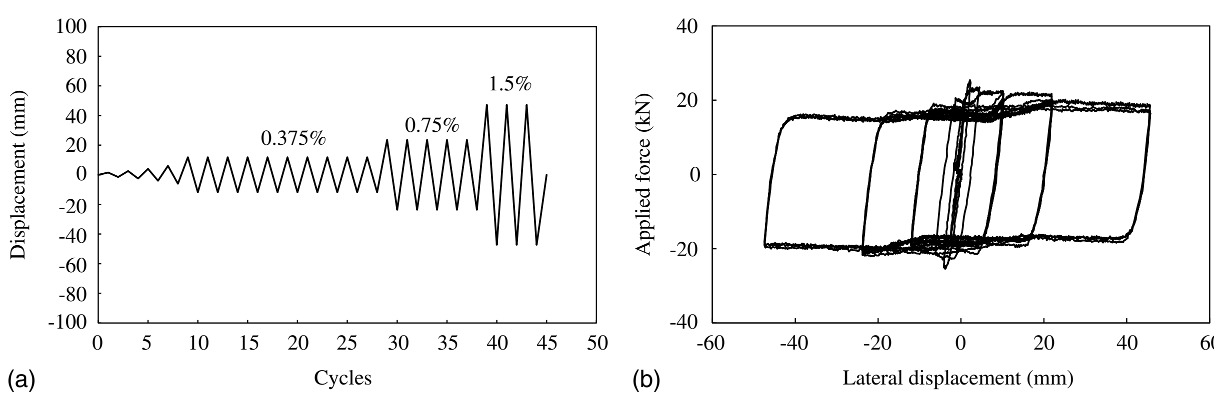

Fig. 7. Hysteresis curve of retrofit system obtained from cyclic loading test: (a) loading protocol; and (b) experimental force-displacement curve.

life safety and collapse prevention performance levels, respectively. The loading protocol used in the test is defined as shown in Fig. 7(a). Fig. 7(b) shows the force-displacement curve of the test structure, where it can be observed that the dampers have a stable behavior and the capacity is approximately 25 kN as estimated by the formulation. However, after a few loading cycles, the yield force is slightly reduced due to the loss of bolt pretension. The torques of the bolts were measured before and after the test, and it was observed that some bolts were loosened during the test. This can be prevented using special washers, or they can be designed with larger torques to be on the safe side. In general, the hysteresis behavior shows a broad loop with a good energy dissipation capability that can be suitable for retrofitting structures. Since there is no displacement at friction faces until the activation moment is reached, except for the elastic deformation of damper elements, it is seen that dampers have a large initial stiffness and show a perfect elastic-plastic behavior.

The behavior of the dampers is further investigated using an analysis model established in OpenSees version 2.5.0 (Mazzoni et al. 2006), the Open System for Earthquake Engineering Simulation. The elements of the installation jig and the links of the dampers are modeled using the force-based nonlinear beam-column elements with fiber sections. The hinges are modeled using two nodes and are pinned together using the *bar* type *rigidLink*, which constrains the translational degrees of freedom. The moment-rotation behavior of the friction faces are defined using the rotational *zerolength* element with the *Hysteretic* material. The model is analyzed using the displacement-controlled method with a step of 0.1 mm, and the results are presented in Fig. 8. The results of the analysis show that the amplification factor and the load-resisting capacity of the system are consistent with the experimental results and the values predicted by the formulas. The amplification factor can be calculated by dividing the hinge rotation of the friction faces in Fig. 8(d) by the drift ratio shown in Fig. 8(c), which is around 5.7, as calculated earlier. The only discrepancy is in the capacity of the system, which is attributed to the loss of bolt pretension observed during the test. Overall, the theoretical, experimental, and analytical results show consistency, and the behavior of the proposed dampers seems suitable for application in the seismic retrofit of existing structures.

Application to an Analysis Model Structure

Structural Details

To evaluate the seismic retrofit capability of the suggested retrofit system, a four-story RC structure with a soft first story is considered as the case study structure, and its seismic performance is evaluated before and after the retrofit. The overall three-dimensional (3D) view of the structure is shown in Fig. 9, and the plan layout is shown in Fig. 10. The height of all stories is $3m$. The first story consists of RC columns and the core wall, and the higher stories are designed with RC load-bearing walls. The structure is one-way asymmetric in the plan owing to the eccentrically located core wall surrounding the staircase. The dead load (DL) and the live load (LL) are assumed

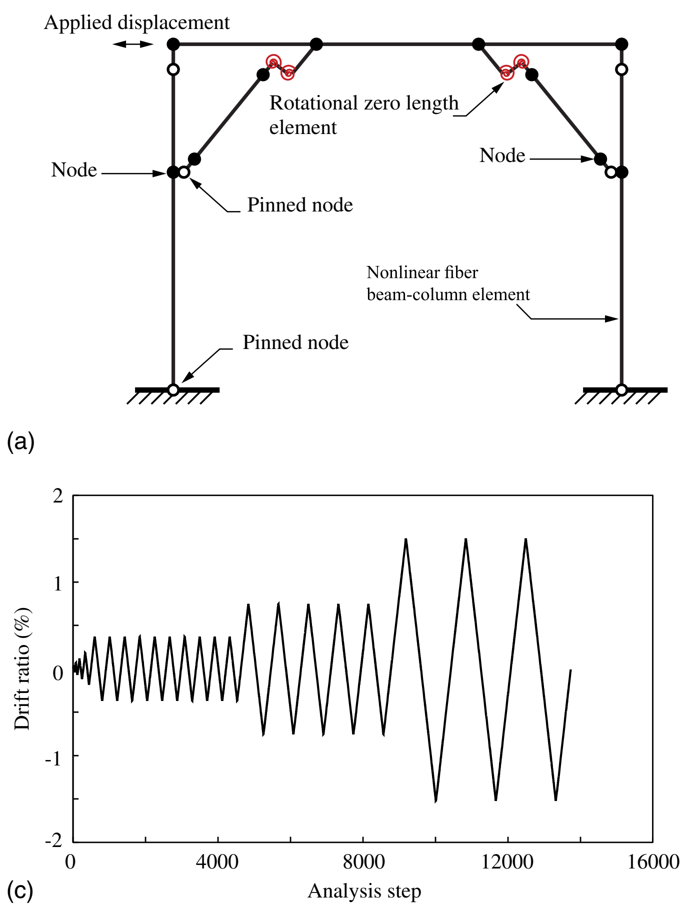

Fig. 8. (a) Analysis model of test structure; (b) force-displacement curve of analysis model; (c) applied lateral displacement; and (d) moment-rotation of friction damper at Hinge B.

J. Struct. Eng., 2019, 145(12): 04019162

to be 600 and 300 kN/m^2, respectively. The compressive strength of the concrete and the yield strength of the steel are considered to be 20 and 400 MPa, respectively. The columns are 400×400 mm in sectional size with 8Ø16 rebars, while the beams on the first story have 2Ø14 rebars at the top and 3Ø14 rebars at the bottom with the same sectional dimensions as the columns. RC load-bearing walls have a thickness of 250 mm and double reinforcement of Ø12@200 mm rebars.

Analysis Modeling

The case study structure is analytically modeled using OpenSees. The beams are modeled using force-based nonlinear beam-column elements with fiber sections. Concrete is modeled using the *Concrete01* model, which is a uniaxial material without tensile strength, and the reinforcing bars are modeled using the Giuffrè-Menegotto-Pinto material model, *Steel02* material. A strain hardening ratio equal to 1% of the initial stiffness is used. To consider shear failure implicitly, the columns are modeled using the concentrated plasticity model (Deierlein et al. 2010), as shown in Fig. 11(a). The fiber model is used along the length of the elements, and the elastic uniaxial material model is applied to the fibers. The nonlinearity is concentrated at the ends using uncoupled nonlinear rotational springs in both horizontal directions. The springs are modeled using the *Hysteretic* material in OpenSees, and the backbone curve with the brittle behavior is defined based on ASCE/SEI 41. To compare the behavior of this model with that of the nonlinear fiber model, a cantilever column is modeled and subjected to an arbitrary cyclic load. Fig. 11(b) shows the hysteretic behaviors of the column modeled with (1) a nonlinear fiber element, (2) an elastic element with nonlinear spring hinges and an idealized bilinear backbone curve, and (3) an elastic element with nonlinear spring hinges and implicit shear failure. It can be observed that the concentrated plasticity model with the idealized bilinear backbone curve can reasonably capture the behavior of the nonlinear fiber element model. In this study the concentrated plasticity model is used, except that the bilinear backbone curve is modified according to ASCE/SEI 41 to capture the behavior of the column with shear failure.

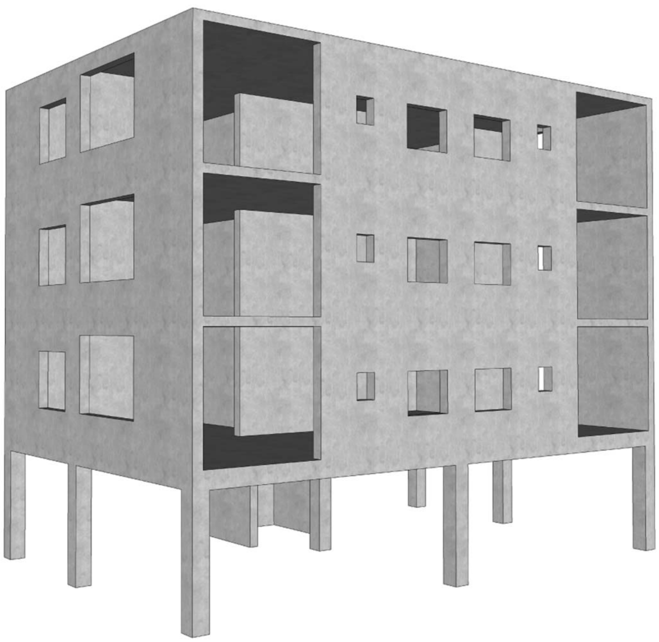

Fig. 9. 3D view of case study structure.

The RC load-bearing walls are modeled using the multilayer shell element in OpenSees. The walls are subdivided into 10 layers, 4 layers for the core concrete, 2 layers for the cover concrete, and 4 layers for the transverse and longitudinal rebars. The force-based nonlinear beam-column element and the multilayer shell element were validated in previous studies, where the efficiency of using macro and micro models was also discussed (Amini et al. 2018; Lu et al. 2015; Shayanfar and Javidan 2017; Usefi et al. 2018). The gravity loads are directly distributed to the beams based on the tributary area, and the rigid diaphragm and a 5% damping ratio are considered in the analysis.

The analysis model contains 11,135 nodes with 6 degrees of freedom, 343 nonlinear beam-column elements with fiber sections, and 10,224 multilayer shell elements with 10 layers. Accordingly, the nonlinear time-history analysis is very costly in terms of the computational time. To increase the computational efficiency, a parallel computing technique is used and the analysis model is divided up and run on 50 processors using the OpenSeesMP interpreter. The nonlinear dynamic analyses are done using a Newmark integrator and adaptive time steps to provide computational efficiency and to avoid convergence problems. The time steps for analysis are

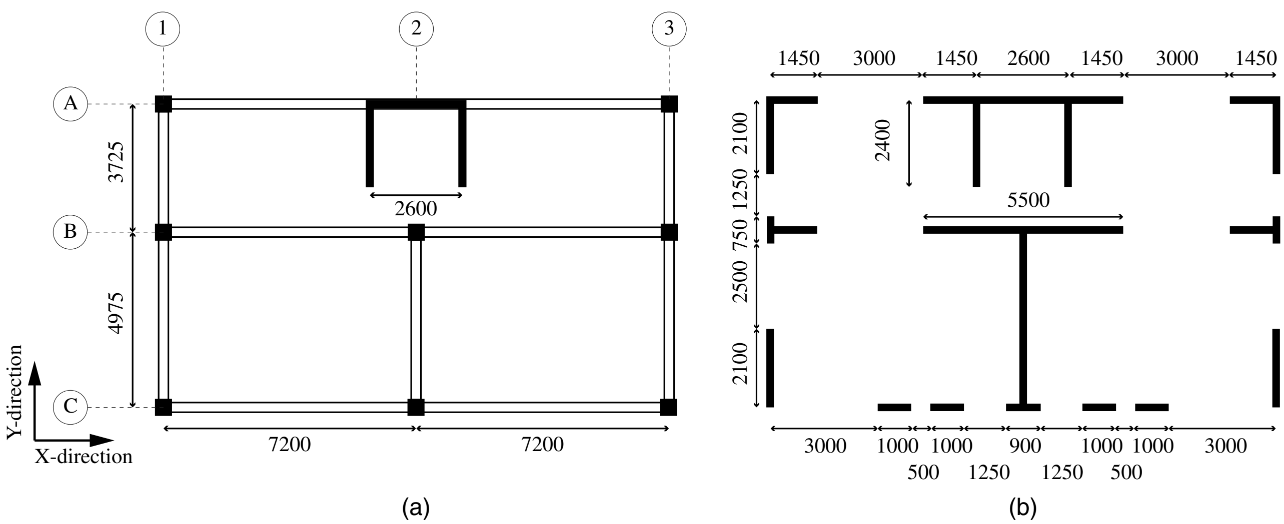

Fig. 10. Plan layout of case study structure: (a) first floor; and (b) second–fourth floors (unit: millimeter).

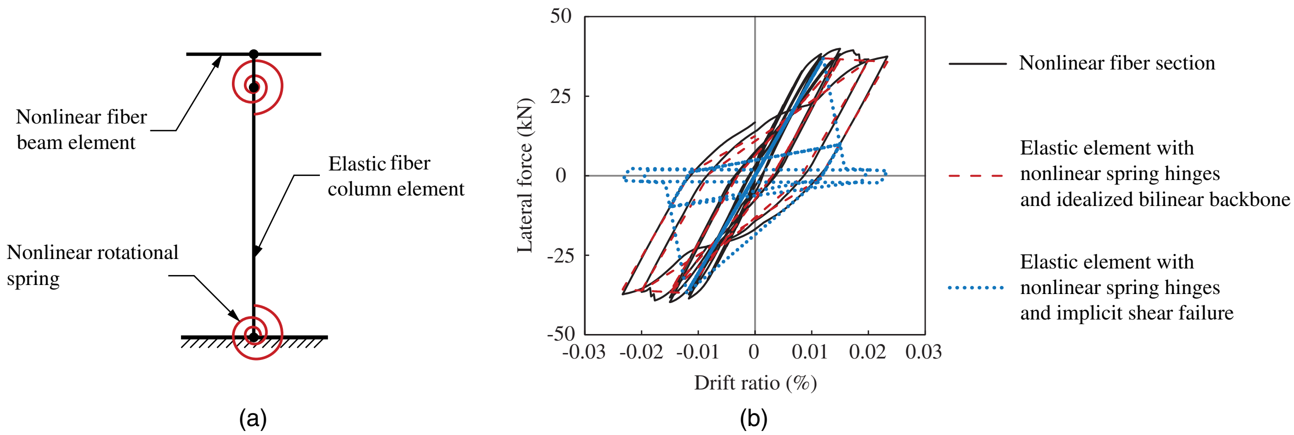

Fig. 11. Analysis model for columns in this study: (a) concentrated plasticity model; and (b) comparison of concentrated plasticity models and fiber model.

initially considered to be equal to the time step of ground motion records; if convergence is not achieved, the time step is halved. In the case of 20 analysis steps with successful convergence, the time step is doubled to increase the computational efficiency.

Seismic Performance of Model Structure

To investigate the seismic performance of the model structure, an eigenvalue analysis is conducted first to find the mode shapes and their corresponding periods for further analysis. The first two mode shapes are shown in Fig. 12, where it can be observed that the structure is highly affected by the torsional irregularity. The torsion is mainly caused by the difference in stiffness at the two sides of the structure, Line A and Line C. The effect of the soft story is also clear in the first mode shape, and as the center of mass is shifted significantly along the x-direction in the first mode, the main damage is expected to occur in the x-direction.

To evaluate the performance of the model structure and the efficiency of the retrofit strategy, seven earthquakes, each containing two horizontal components, are chosen from the PEER NGA

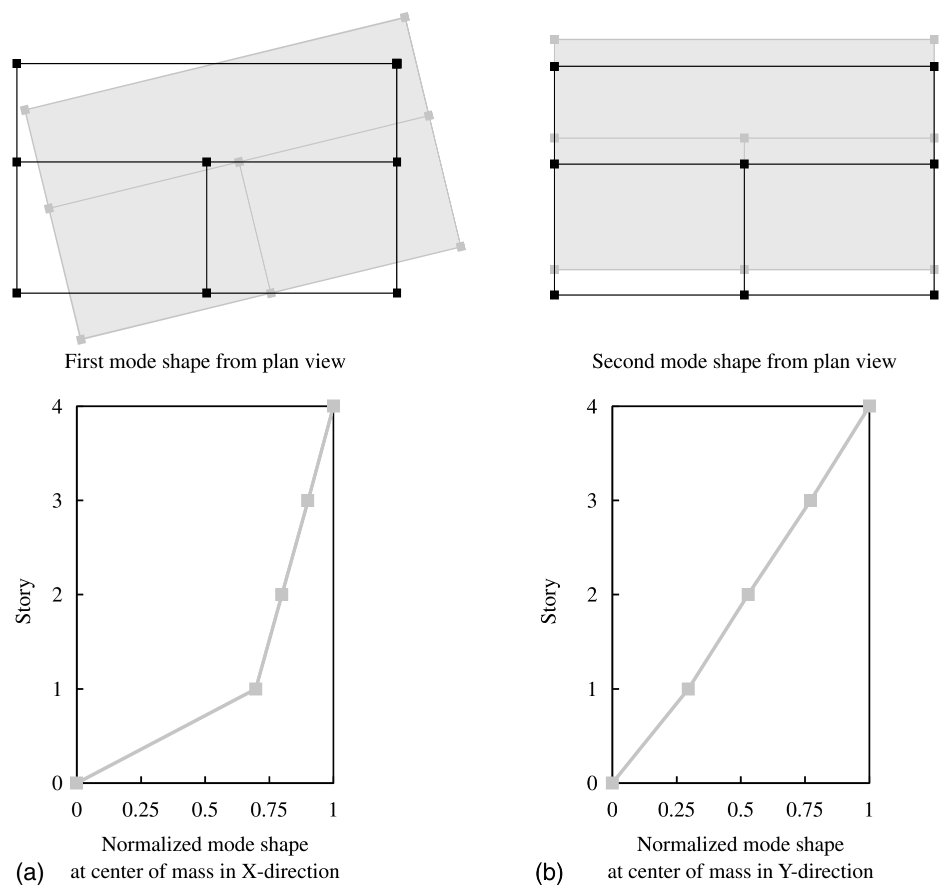

Fig. 12. Results of eigen analysis: (a) first mode shape $T = 0.32$ s; and (b) second mode shape $T = 0.17$ s.

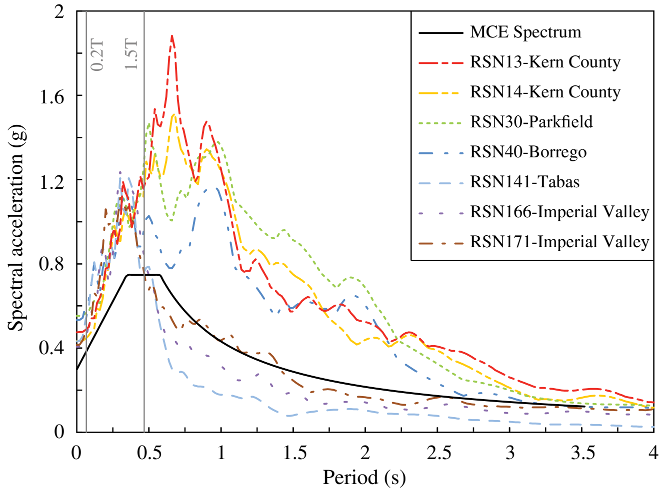

Fig. 13. MCE spectrum and SRSS spectra of seven earthquake ground motions.

database (PEER 2014) and scaled to meet the MCE spectrum of Korea. The MCE spectral response acceleration parameters are $S_{MS} = 0.75g$ for short periods and $S_{M1} = 0.43g$ at a period of 1 s. Each pair of ground motion records is scaled so that its square root of the sum of the squares (SRSS) spectrum does not fall below the MCE spectrum between the period range of $0.2T$ and $1.5T$ (ASCE 2013). The fundamental period of the structure is 0.32 s, and the considered MCE spectrum along with the SRSS spectra of the scaled earthquake ground motions are shown in Fig. 13.

The maximum and average interstory drift ratios of the structure under the seven earthquake ground motions are shown in Fig. 14. The maximum drifts occur at a corner of the flexible edge, and the average drift ratios are computed at the center of mass. The target performance point is set to be the maximum drift ratio of 1% under the MCE ground motions. It is observed that the maximum drift ratios under some ground motions are much larger than the prescribed drift ratios of 1.5%, which corresponds to the collapse prevention performance level according to the Korean seismic code. Maximum interstory drift ratios are larger than the corresponding drift ratios at the center of mass, which signifies the torsional

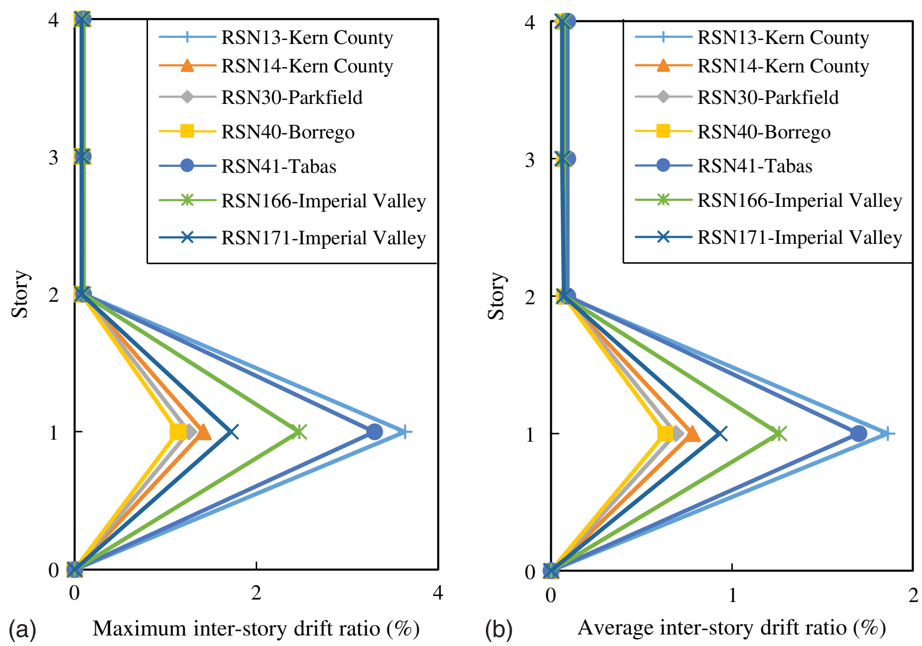

Fig. 14. Seismic responses of model structure before retrofit: (a) Maximum interstory drift ratio (%); and (b) average interstory drift ratio (%).

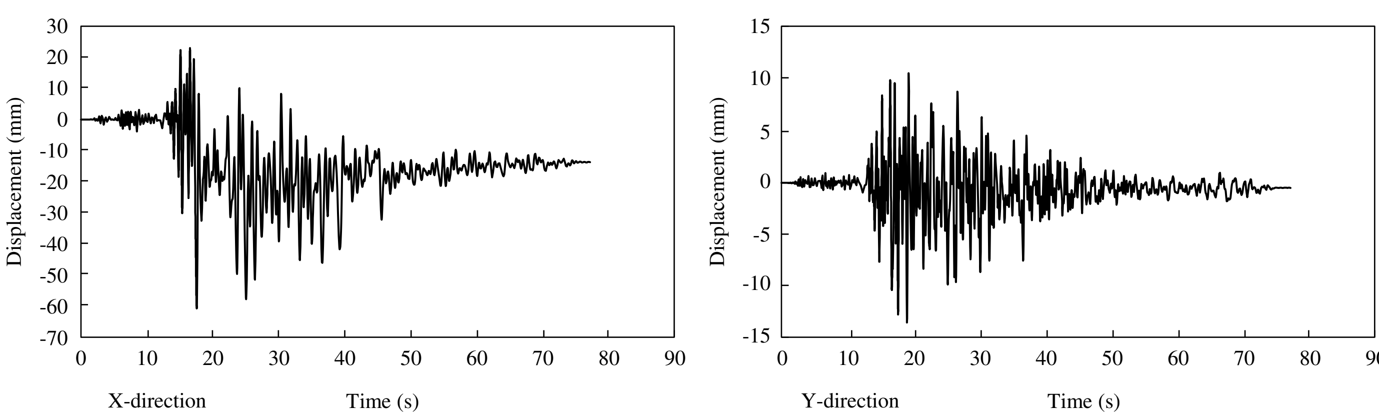

Fig. 15. First-story displacement time history under RSN13-Kern County earthquake.

irregularity of the structure. Moreover, the load-bearing walls above the first story show near rigid body movement, and the seismic responses are concentrated at the soft first story. It can be observed that the maximum drift ratios are larger than 2%, which implies significant damage in the structure. The displacement time history at the center of mass of the first story under the RSN13-Kern County earthquake is depicted in Fig. 15. There are 13.7 and 0.6 mm residual displacements at the center of mass in the x- and y-directions, respectively. Similar behavior is observed for the RSN141-Tabas and RSN166-Imperial Valley earthquakes with maximum drift ratios larger than 2%.

Retrofit of Model Structure

The seismic performance of the model structure is improved using the retrofit system to meet the maximum drift ratio of 1% under the MCE ground motion. To achieve this performance objective, the rotational friction dampers are installed at the two bays along the flexible edge (Line C in Fig. 10). The behavior of the damper is modeled using the *twoNodeLink* elements with the *Hysteretic* material as shown in Fig. 16. The springs are attached to each considered bay in parallel to the nodes of the existing columns. The capacity of the retrofit system is taken to be 50 kN.

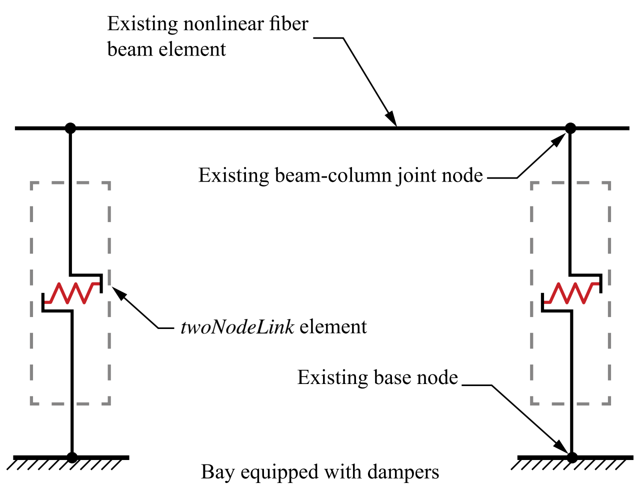

Fig. 16. Macromodel of retrofit system.

The retrofitted structure is analyzed under the seven earthquake ground motions used previously, and the maximum and the average drift ratios are depicted in Fig. 17. It can be seen that the maximum drift ratios decrease considerably after the retrofit, and the largest drift ratios are due to the RSN166-Imperial Valley and the RSN171-Imperial Valley earthquakes, which are equal to 1.7% and 1.2%, respectively. It is also found that the mean value of the maximum interstory drift ratios is limited to 1.0%, which meets the target criterion. The displacement time history under the RSN166-Imperial Valley and RSN13-Kern County earthquakes are compared before and after the retrofit in Fig. 18. It is observed that by implementing the suggested retrofit strategy, the residual displacements also decrease considerably, and the shear failure of columns is prevented. The hysteretic behavior of the dampers acting on each bay under the RSN166-Imperial Valley earthquake is shown in Fig. 19. The dampers attached to the two bays in Line C dissipate seismic energy efficiently, and as a result the drifts in the x-direction are limited to the desired performance level.

Concluding Remarks

In this research the efficiency of a seismic retrofit system consisting of a pin-jointed steel frame and rotational friction dampers was evaluated through theoretical formulation, cyclic loading test, and application to an analysis model structure. The energy dissipation capability of the damper was significantly enhanced by designing its geometry in such a way that its rotation was maximized for a given lateral drift of the structure. The test results of the damping system showed that the dampers were suitable for seismic retrofit of structures in which diagonal bracing-type dampers could not be applied. The seismic retrofit design of an analysis model structure with a soft first story and plan asymmetry showed that the proposed

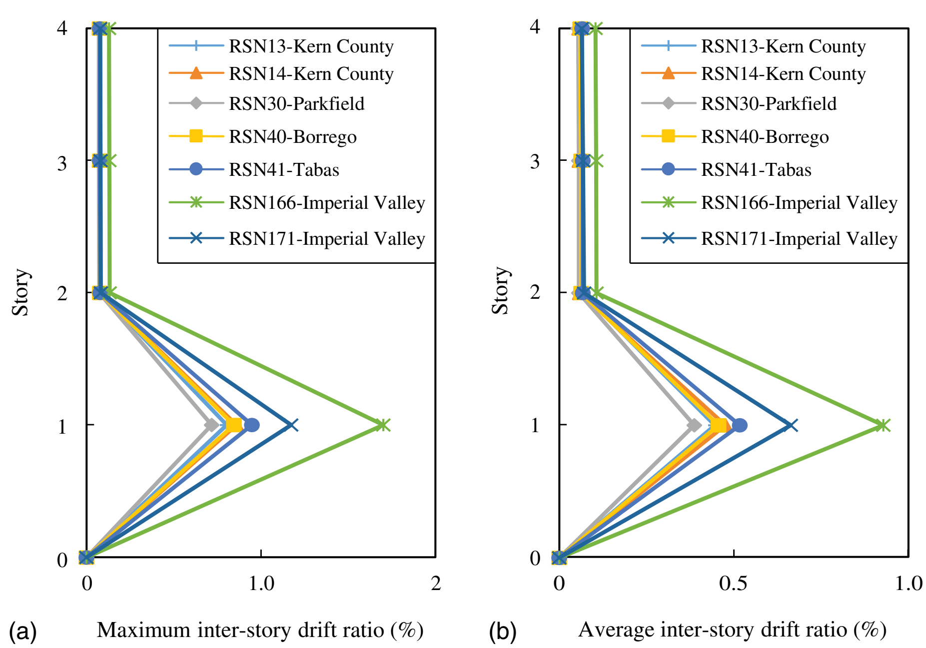

Fig. 17. Seismic responses of model structure after retrofit: (a) maximum interstory drift ratio (%); and (b) average interstory drift ratio (%).

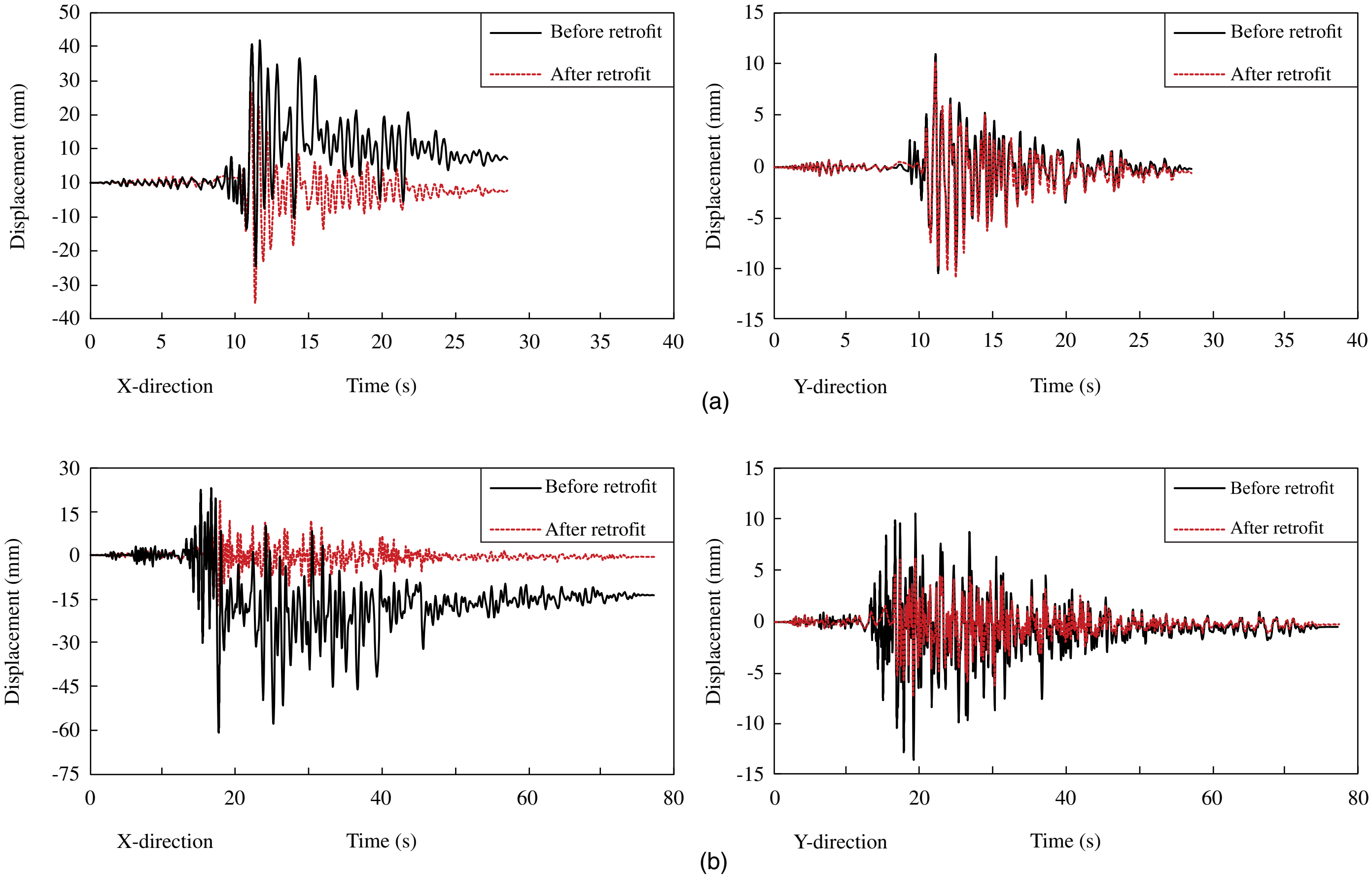

Fig. 18. Comparison between first-story displacement time histories before and after retrofit: (a) RSN166 Imperial Valley earthquake; and (b) RSN13-Kern County earthquake.

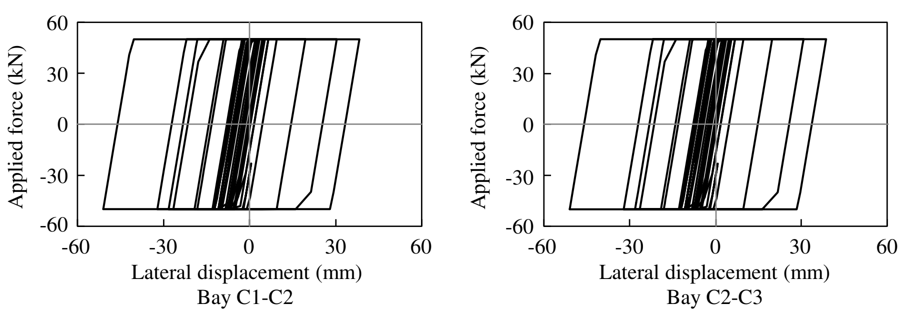

Fig. 19. Hysteresis behavior of dampers under RSN166-Imperial Valley earthquake.

retrofit system could be used efficiently to prevent collapse of the structure and reduce interstory drift ratios below the code-stipulated limit states.

Acknowledgments

This research was supported by Land Transport Technology Promotion Research Project (19CTAP-C153076-01) of the Ministry of Land, Infrastructure and Transport of Korea.

References

Agha Beigi, H., C. Christopoulos, T. Sullivan, and G. M. Calvi. 2014. "Gapped-inclined braces for seismic retrofit of soft-story buildings." *J. Struct. Eng.* 140 (11): 4014080. https://doi.org/10.1061/(ASCE)ST.1943-541X.0001006.

Agha Beigi, H., T. J. Sullivan, C. Christopoulos, and G. M. Calvi. 2015. "Factors influencing the repair costs of soft-story RC frame buildings and implications for their seismic retrofit." *Eng. Struct.* 101 (Oct): 233–245. https://doi.org/10.1016/j.engstruct.2015.06.045.

Amini, F., M. Bitaraf, M. S. Eskandari Nasab, and M. M. Javidan. 2018. "Impacts of soil-structure interaction on the structural control of nonlinear systems using adaptive control approach." *Eng. Struct.* 157 (Feb): 1–13. https://doi.org/10.1016/j.engstruct.2017.11.071.

ASCE. 2013. *Seismic rehabilitation of existing buildings*. ASCE/SEI 41. Reston, VA: ASCE.

Baquero Mosquera, J. S., J. L. Almazán, and N. F. Tapia. 2016. "Amplification system for concentrated and distributed energy dissipation devices." *Earthquake Eng. Struct. Dyn.* 45 (6): 935–956. https://doi.org/10.1002/eqe.2692.

Belleri, A., A. Marini, P. Riva, and R. Nascimbene. 2017. "Dissipating and re-centring devices for portal-frame precast structures." *Eng. Struct.* 150 (Nov): 736–745. https://doi.org/10.1016/j.engstruct.2017.07.072.

Bucher, C. 2009. "Probability-based optimal design of friction-based seismic isolation devices." *Struct. Saf.* 31 (6): 500–507. https://doi.org/10.1016/j.strusafe.2009.06.009.

Deierlein, G., A. Reinhorn, and M. Willford. 2010. *Nonlinear structural analysis for seismic design*. Gaithersburg, MD: National Institute of Standards and Technology.

Hwang, J.-S., Y.-N. Huang, and Y.-H. Hung. 2005. "Analytical and experimental study of toggle-brace-damper systems." *J. Struct. Eng.* 131 (7): 1035–1043. https://doi.org/10.1061/(ASCE)0733-9445(2005)131:7(1035).

Kang, J.-D., and H. Tagawa. 2014. "Experimental evaluation of dynamic characteristics of seesaw energy dissipation system for vibration control of structures." *Earthquake Eng. Struct. Dyn.* 43 (12): 1889–1895. https://doi.org/10.1002/eqe.2420.

Kim, J., and J. Jeong. 2016. "Seismic retrofit of asymmetric structures using steel plate slit dampers." *J. Constr. Steel Res.* 120 (Apr): 232–244. https://doi.org/10.1016/j.jcsr.2016.02.001.

Lee, J., H. Kang, and J. Kim. 2017. "Seismic performance of steel plate slit-friction hybrid dampers." *J. Constr. Steel Res.* 136 (May): 128–139. https://doi.org/10.1016/j.jcsr.2017.05.005.

Lee, J., and J. Kim. 2015. "Seismic evaluation of the performance moment frames with slit-hybrid friction dampers." *Earthquakes Struct.* 9 (6): 1291–1311. https://doi.org/10.12989/eas.2015.9.6.1291.

Lu, X., L. Xie, H. Guan, Y. Huang, and X. Lu. 2015. "A shear wall element for nonlinear seismic analysis of super-tall buildings using OpenSees." *Finite Elem. Anal. Des.* 98 (Jun): 14–25. https://doi.org/10.1016/j.finel.2015.01.006.

Martinelli, P., and M. G. Mulas. 2010. "An innovative passive control technique for industrial precast frames." *Eng. Struct.* 32 (4): 1123–1132. https://doi.org/10.1016/j.engstruct.2009.12.038.

Mazzoni, S., F. McKenna, M. H. Scott, and G. L. Fenves. 2006. *OpenSees command language manual*. Berkeley, California: Univ. of California.

Mualla, I.H., and B. Belev. 2002. "Performance of steel frames with a new friction damper device under earthquake excitation." *Eng. Struct.* 24 (3): 365–371. https://doi.org/10.1016/S0141-0296(01)00102-X.

Naeem, A., M. N. Eldin, J. Kim, and J. Kim. 2017. "Seismic performance evaluation of a structure retrofitted using steel slit dampers with shape memory alloy bars." *Int. J. Steel Struct.* 17 (4): 1627–1638. https://doi.org/10.1007/s13296-017-1227-4.

Naeem, A., and J. Kim. 2018. "Seismic retrofit of a framed structure using damped cable systems." *Steel Compos. Struct.* 29 (3): 287–299.

PEER (Pacific Earthquake Engineering Research). 2014. "PEER NGA Database." Accessed July 15, 2019. https://ngawest2.berkeley.edu/.

Sahoo, D. R., and D. C. Rai. 2013. "Design and evaluation of seismic strengthening techniques for reinforced concrete frames with soft ground story." *Eng. Struct.* 56 (Nov): 1933–1944. https://doi.org/10.1016/j.engstruct.2013.08.018.

Shayanfar, M. A., and M. M. Javidan. 2017. "Progressive collapse-resisting mechanisms and robustness of RC frame–shear wall structures." *J. Perform. Constr. Facil.* 31 (5): 4017045. https://doi.org/10.1061/(ASCE)CF.1943-5509.0001012.

Şigaher, A. N., and M. C. Constantinou. 2003. "Scissor-jack-damper energy dissipation system." *Earthquake Spectra* 19 (1): 133–158.

Usefi, N., H. Ronagh, K. Kildashti, and B. Samali. 2018. "Macro/micro analysis of cold-formed steel members using Abaqus and OpenSees." In *Proc., 13th Int. Conf. on Steel, Space and Composite Structures*. Perth, Australia: Univ. of Western Australia.

Weber, F., J. Distl, L. Meier, and C. Braun. 2018. "Curved surface sliders with friction damping, linear viscous damping, bow tie friction damping, and semiactively controlled properties." *Struct. Control Health Monit.* 25 (11): e2257. https://doi.org/10.1002/stc.2257.

Yousef-Beik, S. M. M., P. Zarnani, F. M. Darani, A. Hashemi, and P. Quenneville. 2018. "New seismic damage avoidant timber brace using innovative resilient slip friction joints for multi-story applications." In *Proc., World Conf. on Timber Engineering*. Helsinki, Finland: Finnish Association of Civil Engineers.

Zhou, Y., and P. Chen. 2017. "Shaking table tests and numerical studies on the effect of viscous dampers on an isolated RC building by friction pendulum bearings." *Soil Dyn. Earthquake Eng.* 100 (Sep): 330–344. https://doi.org/10.1016/j.soildyn.2017.06.002.